Commun. Theor. Phys. **75** (2023) 025102 (13pp) https://doi.org/10.1088/1572-9494/acac1c

Pair production in inhomogeneous electric fields with phase modulation

Li-Na Hu[1], Orkash Amat[1], Lie-Juan Li[1], Melike Mohamedsedik[1] and B S Xie[1,2,*]

[1] Key Laboratory of Beam Technology of the Ministry of Education, and College of Nuclear Science and Technology, Beijing Normal University, Beijing 100875, China
[2] Institute of Radiation Technology, Beijing Academy of Science and Technology, Beijing 100875, China

E-mail: bsxie@bnu.edu.cn

Received 24 October 2022, revised 16 December 2022
Accepted for publication 16 December 2022
Published 6 February 2023

Abstract

Electron-positron pair production in spatial inhomogeneous electric fields with sinusoidal phase modulation is studied within the Dirac-Heisenberg-Wigner formalism. The focus is on discussing the effects of the modulation parameters on the momentum spectrum and the reduced particle number at various spatial scales. For the momentum spectrum, the interference effect becomes more and more remarkable with the increase of modulated amplitude or frequency, while the symmetry is severely destroyed with modulated amplitude. For the reduced particle number, it is greatly enhanced by about a few times and evenly one order of magnitude when modulation parameters are applied. Moreover, the effect of spatial scales on the reduced particle number is carefully examined, and it is found that it increases rapidly at small spatial scales, while it tends to be a constant at large spatial scales. We also obtain the optimal pair production that can be achieved through different modulations. These results can provide a possibility for realizing the optimal pair production by combining the advantages of field spatial inhomogeneity with different choices of phase modulation.

Keywords: electron-positron pair production, Dirac-Heisenberg-Wigner formalism, spatial inhomogeneous fields, phase modulation

(Some figures may appear in colour only in the online journal)

1. Introduction

Electron-positron (e^-e^+) pair production from a vacuum in strong background fields, namely the Sauter-Schwinger effect, is one of the well-known nonperturbative predictions of quantum electrodynamics (QED) [1–4]. It has not been verified experimentally because the current laser intensity $\sim 10^{22}\,\mathrm{W\,cm^{-2}}$ is far less than the critical laser intensity $\sim 10^{29}\,\mathrm{W\,cm^{-2}}$ (the corresponding critical electric field strength is $E_{\mathrm{cr}} = m^2c^3/e\hbar \approx 1.3 \times 10^{16}\,\mathrm{V/cm}$, where m denotes the electron mass and e is the magnitude of electron charge) [5, 6]. Multiphoton pair production is also served as an important mechanism for e^-e^+ pair creation, which has been detected in the laboratory [7, 8]. Moreover, the pair production can be observed even in the laser field with intensities one or two orders of magnitude lower than the critical value [9, 10]. This attributes to the proposed dynamically assisted Schwinger mechanism that combines two laser fields with a low-frequency strong field and a high-frequency weak field [11–16]. Fortunately, with the advance in high-intensity laser technology, the Extreme Light Infrastructure (ELI) [17] and the x-ray free electron laser (XFEL) may achieve subcritical laser intensity, which greatly improves the hope to observe the pair production in the laboratory.

Theoretically, several field configurations have been applied to the study of vacuum pair production, such as the alternating electric field with N-pulse [18], time delay electric field [19], polarized electric field [20, 21], the combination of cosine with Gaussian or super-Gaussian pulse external field [22–27], and so on. Recent studies suggest that the fields with frequency chirp are crucial to the e^-e^+ pair production. It can

* Author to whom any correspondence should be addressed.

not only significantly enhance the total particle number but also achieve experimental verification by applying the chirped pulse amplification (CPA) technique [28]. At present, the asymmetrical [29–32] and symmetrical [33, 34] frequency chirp have been studied on pair production in both spatially homogeneous and inhomogeneous fields. Moreover, sinusoidal frequency modulation has been used in the investigation of pair production in a homogeneous electric field and indicated that the momentum distribution and the number density of created particles are sensitive to modulation parameters [35].

Moreover, the previous investigations show that the spatial inhomogeneity of external fields plays an important role in the e^-e^+ pair production, which has displayed some novel effects [36–40]. For example, the self-bunching effect of particles is identified in Schwinger pair production under an electric field with finite spatial scales [37]. The ponderomotive force effect is reported in the multiphoton process for the small spatial scales of an oscillating field [38]. The spin-field interaction is found in Schwinger pair production for spatially inhomogeneous external fields [39]. However, sinusoidal frequency modulation has not been considered in e^-e^+ pair production in spatially inhomogeneous fields. Therefore, it is necessary to explore the vacuum pair creation in inhomogeneous fields with sinusoidal frequency modulation.

In this work, we use real-time Dirac-Heisenberg-Wigner (DHW) formalism to investigate e^-e^+ pair production in spatially inhomogeneous electric fields with sinusoidal phase modulation. The momentum spectrum and the reduced particle number of the created pairs are studied and are found to depend strongly on the amplitude and frequency of the modulated phase. Furthermore, we note that the interference effect and symmetry of the momentum spectrum are obviously changed by applying different modulation parameters. The reduced particle number can also be significantly enhanced by the modulated amplitude, while it has different variations of modulated frequency for different spatial scales. It is evident that the enhanced particle number is achieved by large modulated frequency at small spatial scales, however, at large spatial scales, it is achieved by a small frequency. Moreover, the effect of spatial scale on the reduced particle number is examined. Two interesting features are revealed in the reduced particle number, i.e., the optimal modulation parameters are found and the same particle number can be achieved through different sets of modulation parameters. Meanwhile, some typical interference patterns on the momentum spectrum can be quantitatively understood by bridging momentum peaks and the frequency spectrum of a time-dependent electric field with phase modulation. It is found that the momentum peaks are determined by the pair generation process of absorbing different frequency component photons. Finally, some typical numerical results obtained by the DHW formalism are compared with those obtained by the trajectory-based semiclassical analysis [36, 38, 41] and the local density approximation (LDA) [31, 37, 42], and it is found that the results are in good agreement. Note that the natural units $\hbar = c = 1$ are applied and all quantities are presented in terms of the electron mass m. For example, the spatial and temporal scales of the electric field are in units of $1/m$, and the field frequency is in units of m.

The paper is structured as follows. In section 2, we review the DHW formalism and introduce the background field to be considered in our work. In section 3, the numerical results for different modulation parameters are presented with a physics discussion. Subsection 3.1 and subsection 3.2 show the momentum spectrum and the reduced particle number, respectively. The conclusion and outlook are given in section 4.

2. Theoretical formalism and field model

The DHW formalism is a relativistic phase-space method that has been widely used to investigate vacuum pair creation within arbitrary electromagnetic fields. Since the complete derivation of DHW formalism has been obtained in [31, 37, 43, 44], we only present key points of this method.

We start with the quantum electrodynamics (QED) Lagrangian

$$\mathcal{L}(\Psi, \bar{\Psi}, A) = \frac{1}{2}(\mathrm{i}\bar{\Psi}\gamma^\mu\mathcal{D}_\mu\Psi - \mathrm{i}\bar{\Psi}\mathcal{D}_\mu^\dagger\gamma^\mu\Psi) - m\bar{\Psi}\Psi - \frac{1}{4}F_{\mu\nu}F^{\mu\nu}, \tag{1}$$

where $\mathcal{D}_\mu = (\partial_\mu + \mathrm{i}eA_\mu)$ and $\mathcal{D}_\mu^\dagger = (\overleftarrow{\partial_\mu} - \mathrm{i}eA_\mu)$ denote the covariant derivatives with a vector potential A_μ that vanishes at asymptotic times, and γ^μ represents the gamma matrices. To describe the dynamics of created pairs, we proceed by calculating the Dirac equation

$$(\mathrm{i}\gamma^\mu\partial_\mu - e\gamma^\mu A_\mu - m)\Psi = 0, \tag{2}$$

and the adjoint Dirac equation

$$\bar{\Psi}(\mathrm{i}\overleftarrow{\partial_\mu}\gamma^\mu + e\gamma^\mu A_\mu + m) = 0. \tag{3}$$

The backbone of DHW formalism is the gauge-covariant density operator which is composed of two commutative Dirac field operators, i.e.,

$$\hat{\mathcal{C}}_{\alpha\beta}(r, s) = \mathcal{U}(A, r, s)\,[\bar{\psi}_\beta(r - s/2), \psi_\alpha(r + s/2)], \tag{4}$$

where $r = (r_1 + r_2)/2$ denotes the center-of-mass coordinate and $s = r_1 - r_2$ represents the relative coordinate. The Wilson line factor

$$\mathcal{U}(A, r, s) = \exp\left(\mathrm{i}e\int_{-1/2}^{1/2}\mathrm{d}\xi\, A(r + \xi s)s\right), \tag{5}$$

can be used to guarantee the invariant of the density operator. To obtain a proper phase-space formalism, we perform a Fourier transform of equation (4) from s-space to p-space, which leads to the covariant Wigner operator

$$\hat{\mathcal{W}}_{\alpha\beta}(r, p) = \frac{1}{2}\int \mathrm{d}^4 s\; \mathrm{e}^{\mathrm{i}ps}\,\hat{\mathcal{C}}_{\alpha\beta}(r, s), \tag{6}$$

which is properly defined in terms of four-position r and four-momentum p coordinates. We can combine the Wigner operator (6) with equations (2) and (3) to generate the

operator equations

$$\left(\frac{1}{2}\hat{D}_\mu - \mathrm{i}\hat{P}_\mu\right)\gamma^\mu\hat{\mathcal{W}}(r,p) = -\mathrm{i}m\hat{\mathcal{W}}(r,p), \tag{7}$$

$$\left(\frac{1}{2}\hat{D}_\mu + \mathrm{i}\hat{P}_\mu\right)\hat{\mathcal{W}}(r,p)\gamma^\mu = \mathrm{i}m\hat{\mathcal{W}}(r,p), \tag{8}$$

with the pseudodifferential operators

$$\hat{D}_\mu = \partial^r_\mu - e\int_{-1/2}^{1/2}\mathrm{d}\xi\ \hat{F}_{\mu\nu}(r - \mathrm{i}\xi\partial^p)\partial^\nu_p, \tag{9}$$

$$\hat{P}_\mu = p_\mu - \mathrm{i}e\int_{-1/2}^{1/2}\mathrm{d}\xi\ \xi\ \hat{F}_{\mu\nu}(r - \mathrm{i}\xi\partial^p)\partial^\nu_p. \tag{10}$$

In order to obtain computational feasible equations of motion, we take the vacuum expectation value of equations (7) and (8). At this point, we introduce a mean-field (Hartree) approximation

$$\langle\Phi|\hat{F}^{\mu\nu}(r)|\Phi\rangle \approx F^{\mu\nu}(r). \tag{11}$$

The electromagnetic field strength tensor $\hat{F}^{\mu\nu}$ is treated as a C-number valued function $F^{\mu\nu}$. This approximation becomes apparent when we consider terms of the form $\langle\hat{F}^{\mu\nu}(r)\ \hat{\mathcal{C}}(r,s)\rangle$, which can be expressed as

$$\langle\Phi|\hat{F}^{\mu\nu}(r)\ \hat{\mathcal{C}}(r,s)|\Phi\rangle \approx F^{\mu\nu}(r)\langle\Phi|\hat{\mathcal{C}}(r,s)|\Phi\rangle. \tag{12}$$

Consequently, equations (7) and (8) are transformed into equations of motion for the covariant Wigner function

$$\mathbb{W}(r,p) = \langle\Phi|\hat{\mathcal{W}}(r,p)|\Phi\rangle. \tag{13}$$

For the convenience of numerical calculations, we decompose the Wigner function using a complete basis set $\{\mathbb{1}, \gamma_5, \gamma^\mu, \gamma^\mu\gamma_5, \sigma^{\mu\nu} =: \frac{\mathrm{i}}{2}[\gamma^\mu, \gamma^\nu]\}$ into 16 covariant Wigner components

$$\mathbb{W} = \frac{1}{4}(\mathbb{1}\mathbb{S} + \mathrm{i}\gamma_5\mathbb{P} + \gamma^\mu\mathbb{V}_\mu + \gamma^\mu\gamma_5\mathbb{A}_\mu + \sigma^{\mu\nu}\mathbb{T}_{\mu\nu}), \tag{14}$$

where $\mathbb{S}$, $\mathbb{P}$, $\mathbb{V}_\mu$, $\mathbb{A}_\mu$ and $\mathbb{T}_{\mu\nu}$ denote scalar, pseudoscalar, vector, axial vector, and tensor, respectively. Since we are dealing with e^-e^+ pair production, and we want to describe it as an initial value problem, the equal-time Wigner function can be obtained by taking the energy average of the covariant Wigner function

$$\mathbb{w}(\boldsymbol{x},\boldsymbol{p},t) = \int\frac{\mathrm{d}p_0}{2\pi}\ \mathbb{W}(r,p). \tag{15}$$

Combining the above, we eventually obtain a partial differential equations system for the 16 equal-time Wigner function as

$$D_t\mathbb{s} - 2\boldsymbol{\Pi}\cdot\mathbb{t}_1 = 0, \tag{16}$$

$$D_t\mathbb{p} + 2\boldsymbol{\Pi}\cdot\mathbb{t}_2 = -2m\mathbb{a}_0, \tag{17}$$

$$D_t\mathbb{v}_0 + \boldsymbol{D}\cdot\mathbb{v} = 0, \tag{18}$$

$$D_t\mathbb{a}_0 + \boldsymbol{D}\cdot\mathbb{a} = 2m\mathbb{p}, \tag{19}$$

$$D_t\mathbb{v} + \boldsymbol{D}\ \mathbb{v}_0 + 2\boldsymbol{\Pi}\times\mathbb{a} = -2m\mathbb{t}_1, \tag{20}$$

$$D_t\mathbb{a} + \boldsymbol{D}\ \mathbb{a}_0 + 2\boldsymbol{\Pi}\times\mathbb{v} = 0, \tag{21}$$

$$D_t\mathbb{t}_1 + \boldsymbol{D}\times\mathbb{t}_2 + 2\boldsymbol{\Pi}\ \mathbb{s} = 2m\mathbb{v}, \tag{22}$$

$$D_t\mathbb{t}_2 - \boldsymbol{D}\times\mathbb{t}_1 - 2\boldsymbol{\Pi}\ \mathbb{p} = 0, \tag{23}$$

where $\mathbb{t}_1 = 2\mathbb{t}^{i0}\boldsymbol{e}_i$ and $\mathbb{t}_2 = \epsilon_{ijk}\mathbb{t}^{jk}\boldsymbol{e}_i$. The pseudodifferential operators are given by

$$D_t = \partial_t + e\int\mathrm{d}\xi\boldsymbol{E}(\boldsymbol{x} + \mathrm{i}\xi\boldsymbol{\nabla}_p, t)\cdot\boldsymbol{\nabla}_p, \tag{24}$$

$$\boldsymbol{D} = \boldsymbol{\nabla}_x + e\int\mathrm{d}\xi\boldsymbol{B}(\boldsymbol{x} + \mathrm{i}\xi\boldsymbol{\nabla}_p, t)\times\boldsymbol{\nabla}_p, \tag{25}$$

$$\boldsymbol{\Pi} = \boldsymbol{p} - \mathrm{i}e\int\mathrm{d}\xi\xi\boldsymbol{B}(\boldsymbol{x} + \mathrm{i}\xi\boldsymbol{\nabla}_p, t)\times\boldsymbol{\nabla}_p. \tag{26}$$

For a (1+1)-dimensional electromagnetic field with vanishing magnetic field $A_\mu(\boldsymbol{r},t) = (0,0,0,-A_x(x,t)/c)$ where $E_x(x,t) = -\partial A_x(x,t)/(c\partial t)$, the equation (14) can be reduced to the following form

$$\mathbb{W} = \frac{1}{4}(\mathbb{1}\mathbb{S} + \mathrm{i}\gamma_5\mathbb{P} + \gamma^\mu\mathbb{V}_\mu). \tag{27}$$

Therefore, the DHW equations of motion in QED_{1+1} are described as

$$D_t\mathbb{s} - 2p_x\mathbb{p} = 0, \tag{28}$$

$$D_t\mathbb{v}_0 + \partial_x\mathbb{v}_x = 0, \tag{29}$$

$$D_t\mathbb{v}_x + \partial_x\mathbb{v}_0 = -2m\mathbb{p}, \tag{30}$$

$$D_t\mathbb{p} + 2p_x\mathbb{s} = 2m\mathbb{v}_x, \tag{31}$$

with

$$D_t = \partial_t + e\int_{-1/2}^{1/2}\mathrm{d}\xi\ E_x(x + \mathrm{i}\xi\partial_{p_x}, t)\partial_{p_x}. \tag{32}$$

The corresponding vacuum initial conditions are

$$\mathbb{s}_{\mathrm{vac}} = -\frac{2m}{\Omega}, \quad \mathbb{v}_{\mathrm{vac}} = -\frac{2p_x}{\Omega}, \tag{33}$$

where Ω represents the one-particle energy, which can be expressed as $\Omega = \sqrt{p_x^2 + m^2}$. By subtracting these vacuum terms, the modified Wigner component can be written as

$$\mathbb{w}^v_k(x,p_x,t) = \mathbb{w}_k(x,p_x,t) - \mathbb{w}_{k\ \mathrm{vac}}(p_x), \tag{34}$$

here $\mathbb{w}_k$ is the Wigner component in equations (28)–(31) (with the correspondence: $\mathbb{w}_0 = \mathbb{s}$, $\mathbb{w}_1 = \mathbb{v}_0$, $\mathbb{w}_2 = \mathbb{v}_x$ and $\mathbb{w}_3 = \mathbb{p}$). The $\mathbb{w}_{k\ \mathrm{vac}}$ denotes the corresponding vacuum initial condition in equation (33). The particle number density in the phase space can be expressed as

$$n(x,p_x,t) = \frac{m\mathbb{s}^v(x,p_x,t) + p_x\mathbb{v}^v_x(x,p_x,t)}{\Omega(p_x)}. \tag{35}$$

We can obtain the momentum distribution function via integrating equation (35) with respect to x,

$$n(p_x,t) = \int\mathrm{d}x\ n(x,p_x,t). \tag{36}$$

Consequently, the total particle yield of the whole phase space can be written as

$$N(t) = \int\mathrm{d}x\ \mathrm{d}p_x n(x,p_x,t). \tag{37}$$

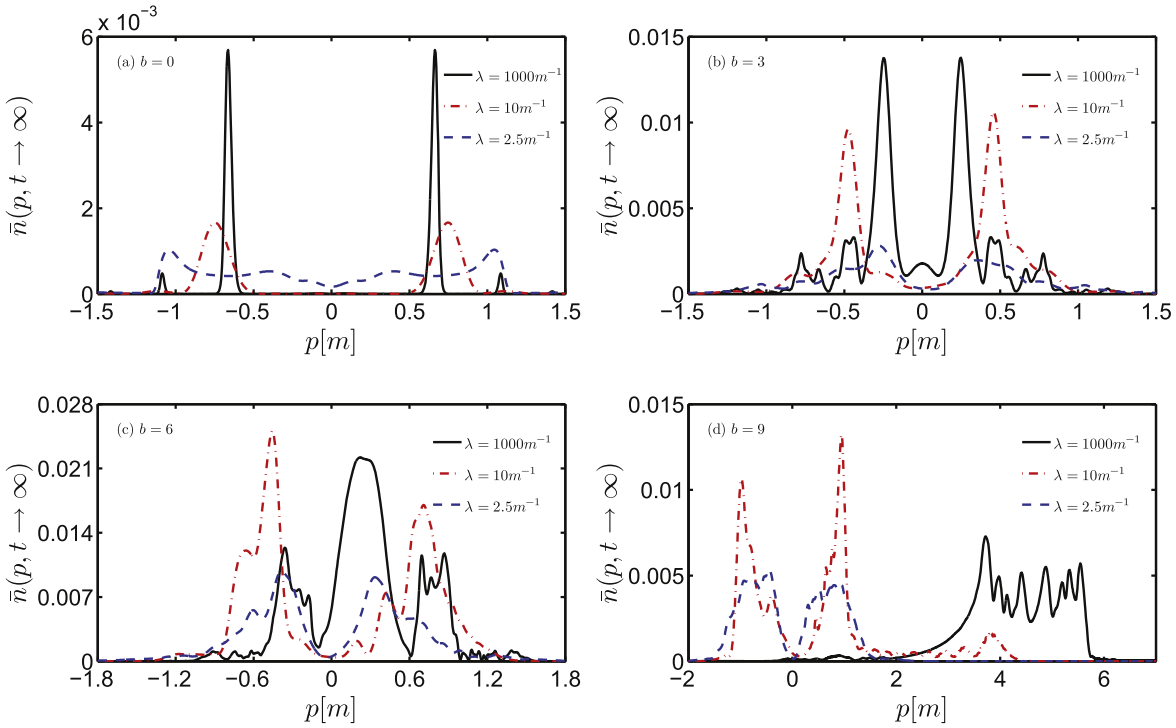

Figure 1. Reduced momentum spectrum for various modulated amplitude values in an electric field (38) with different spatial scales when the modulated frequency is $\omega_m = 0.05$. The modulated amplitude values are $b = 0$, 3, 6 and 9, respectively. Other field parameters are $E_0 = 0.3E_{\rm cr}$, $\omega = 0.5$, $\tau = 100$.

Moreover, in order to extract the nontrivial effect of spatial scale λ, we calculate the reduced quantities $\bar{n}(p_x, t) \equiv n(p_x, t)/\lambda$ and $\bar{N}(t \to \infty) \equiv N(t \to \infty)/\lambda$.

2.1. Model for the external field

We investigate pair production in (1+1)-dimensional spatially inhomogeneous electric field with sinusoidal phase modulation, where the field model can be described as [35]

$$\begin{aligned} E(x, t) &= E_0 f(x) g(t) \\ &= E_0 \exp\left(-\frac{x^2}{2\lambda^2}\right) \exp\left(-\frac{t^2}{2\tau^2}\right) \cos(\omega t + b \sin(\omega_m t)), \end{aligned} \tag{38}$$

where E_0 denotes the field strength, λ is the spatial scale, τ is the pulse duration, ω represents the central frequency, b and ω_m are the amplitude and frequency of the phase modulation, respectively. The nonzero modulated frequency ω_m and modulated amplitude b lead to the time-dependent effective frequency $\omega_{\rm eff}(t) = \omega + b\omega_m \cos(\omega_m t)$. In order to keep the modulation within a reasonable range, we set $|b\omega_m \cos(\omega_m t)| \leqslant \alpha\omega$ with $0 < \alpha < 1$. Because of $|b\omega_m \cos(\omega_m t)|_{\max} = b\omega_m$, the inequality $b\omega_m \leqslant \alpha\omega$ can be derived. We can further obtain the relationship $b \leqslant \alpha\omega/\omega_m$, which also indicates that the upper and lower limits of the modulated amplitude can be obtained. Without losing the generality, we select the regime of $0 \leqslant \alpha \leqslant 0.9$ and the modulated frequency $\omega_m \approx (1/5 \sim 1/10)\omega$, meanwhile, it is noted that when we choose the maximum modulated amplitude, the minimum modulated frequency is considered, i.e., $\omega_m = \omega/10$. In our numerical study, the field parameters are set as $E_0 = 0.3E_{\rm cr}$, $\omega = 0.5$, $\tau = 100$, therefore the corresponding maximum values of modulated amplitude and frequency can be selected as $b = 0.9\omega/\omega_m = 9$ and $\omega_m = \omega/5 = 0.1$, respectively.

The external field in equation (38) is considered as the simplified model for the colliding laser pulses in the standing wave profile with finite extension. Moreover, since particles are mainly created along the electric field direction, by ignoring the particle motion orthogonal to the dominant electric field direction, the system is reduced to the (1+1) dimension [37, 38, 40].

3. Numerical results

In this section, we investigate the effects of sinusoidal phase modulation on the momentum spectrum and the reduced particle number of the created particles in an inhomogeneous field. The field parameters are set as $E_0 = 0.3E_{\rm cr}$, $\omega = 0.5$, $\tau = 100$, which corresponds to the multiphoton-dominant pair production process.

3.1. Momentum spectrum

We first study the influence of the modulated amplitude and frequency on the momentum spectrum for various spatial scales, respectively.

3.1.1. Modulated amplitude. When the modulated frequency is fixed $\omega_m = 0.1\omega = 0.05$, the momentum spectrum for different spatial scales with various modulated amplitude

Table 1. The odd/even property, i.e., $-/+$ sign presentation, of the physical quantity under time reversal.

physical quantity	$(t,\ p_x,\ x,\ \Omega,\ E)$	$(\partial_t,\ \partial_{p_x},\ \partial_x,\ D_t)$	$(\mathbb{s},\ \mathbb{v}_1,\ \mathbb{p},\ \mathbb{v}_0)$
$-/+$	$(-,\ -,\ +,\ +,\ +)$	$(-,\ -,\ +,\ -)$	$(+,\ -,\ +,\ +)$

b is shown in figure 1. At the large spatial scale $\lambda = 1000$, when $b = 0$, we find that the momentum peak presents good monotonicity and the momentum spectrum is symmetrical, as shown in figure 1(a). Since in the quasihomogeneous limit, i.e., $\lambda = 1000$, the electric field model proposed in equation (38) can be written as an even function with only time dependence, i.e., $E(x,\ t) \approx E(t) = E(-t)$, which leads to the symmetry of the momentum spectrum. Actually, this symmetry is due to the fact that the DHW equations for getting the momentum distribution function are invariant under time reversal. Under time reversal, the time t, and the momentum p_x change sign, the x does not change sign. Because $\Omega(-p_x) = \sqrt{(-p_x)^2 + m^2} = \Omega(p_x)$, we can know from equation (33) that $\mathbb{s}^v(x,\ p_x,\ t) = \mathbb{s}^v(x,\ -p_x,\ -t)$ and $\mathbb{v}_1^v(x,\ p_x,\ t) = -\mathbb{v}_1^v(x,\ -p_x,\ -t)$. At the same time, the odd/even property of other physical quantities that affect the momentum distribution function can be obtained by equations (32) and (28)–(31) as shown in table 1. Finally, it is found that the form of the DHW equations stays invariant under time reversal, which ensures the symmetry of the momentum spectrum.

For small modulated amplitude, the momentum spectrum is approximately symmetrical and presents an obvious oscillation, as shown in figure 1(b). Since the effective frequency of the external field $\omega_{\text{eff}}(t) = \omega + b\omega_m \cos(\omega_m t)$ increases significantly with the modulation amplitude, resulting in the enhancement of oscillation. It implies that there is a remarkable interference effect on the momentum spectrum. Meanwhile, the interference effect can be qualitatively understood by the semiclassical Wentzel-Kramers-Brillouin (WKB) approach [45–48], i.e., the greater the pair number of turning points closest to the real t axis, the stronger the interference effect [26, 35, 49]. For large modulated amplitude, one can see the strong oscillations on the momentum spectrum and the merger of the two dominant peaks in figures 1(c) and (d), which indicates that the monotonicity of the momentum peak becomes weaker. Moreover, the symmetry of the momentum spectra is severely destroyed. Since when the modulated amplitude is large, the electric field exhibits high amplitude so that the degree of spatial quasihomogeneous is reduced, i.e., the validity of $E(x,\ t) \approx E(t)$ is being lost more and more, which results in the symmetry of the momentum spectrum being destroyed.

When the spatial scale decreases to $\lambda = 10$, for $b = 0$, the momentum spectrum has no obvious oscillation but is approximately symmetrical, while for small modulation amplitude, this symmetry is destroyed, as shown in figures 1(a) and (b). Because the finite spatial scale of the electric field prevents particle production from being dominated by the temporal pulse structure, there is asymmetry in the momentum spectrum. For large modulated amplitude, we can observe that the momentum spectra exhibit strong oscillations and obvious asymmetry in figures 1(c) and (d), meanwhile, the momentum distribution range is broadened. Since the finite laser pulse seems to prevent the coherent superposition of the particle trajectory, and the corresponding interference pattern is disturbed, there is a broadening of the momentum distribution.

At the extremely small spatial scale $\lambda = 2.5$, when $b = 0$, the weak oscillation occurs on the momentum spectrum, meanwhile, an approximate symmetry can be observed, as shown in figure 1(a). The influence of the electric field focusing on the small spatial scale is so small that equation (32) can be written as $D_t \approx \partial_t$. At the same time, it is found that the odd/even property of physical quantities that affect the momentum spectrum under time reversal is the same as those in table 1. Therefore, the form of the DHW equations still stays invariant, which leads to an approximate symmetry of the momentum spectrum. With increasing modulated amplitude, one can see that the symmetry is gradually destroyed because the validity of $D_t \approx \partial_t$ is being lost more and more. On the other hand, however, obvious oscillations appear in the momentum spectra, as shown in figures 1(b), (c), and (d).

In order to compare with the results that we obtained by DHW formalism, the trajectory-based semiclassical analysis approach [36, 38, 41] and the LDA method are introduced [31, 37, 42]. Since we are primarily interested in the momentum spectrum when the field is turned off, the interaction between the field and particles needs to be considered. The simplest way to achieve this description is to employ a single-trajectory formalism, where electrons/positrons are considered as semiclassical pointlike particles, which follow the classical path [36]. To exclude any kind of interaction between the created particles, these trajectories can be tracked and evaluated. Based on the works in [36, 39, 50, 51], the semiclassical formalism can be written as

$$\frac{\partial x}{\partial t} = \frac{p_x(t)}{\gamma(t)}, \tag{39}$$

$$\frac{\partial p_x}{\partial t} = eE(t,\ x(t)) = eE_0 \exp\left(-\frac{x^2}{2\lambda^2}\right) \times \exp\left(-\frac{t^2}{2\tau^2}\right)\cos(\omega t + b\sin(\omega_m t)), \tag{40}$$

with the Lorentz factor $\gamma(t) = \sqrt{1 + p_x^2}$. It is well known that the momentum has obvious temporal dependence $p_x(t) = A(t_0) - A(t)$, so we bring initial momentum $p_{x,0}$ into the Lorentz force equation, and the momentum at final times $p_{x,f}$ can be obtained by time evolution. Table 2 shows the typical trajectory analyses of particles with different initial momentums. Note that for the convenience of the study, these

Table 2. Trajectory analysis of particles within a spatially inhomogeneous electric field. The results are obtained by solving the relativistic Lorentz force equation for particles seeded at $t_0 = 0$, $x_0 = 0$ in a field of $E_0 = 0.3E_{\rm cr}$, $\omega = 0.5$, $\tau = 100$ and spatial scale λ. The initial momentum $p_{x,0}$ as well as spatial scale λ have been varied. Note that the upper part of table shows the results for $b = 0$, the lower part of table shows the results for $b = 3$. The final momenta $p_{x,f}$ are obtained at asymptotic times. For comparison we provide the results by the DHW calculation $p_{\rm DHW}$.

$\lambda[m^{-1}]$	$p_{x,0}[m]$	$p_{x,f}[m]$	$p_{\rm DHW}[m]$
1000	0.664	0.664	0.664
10	0.664	0.756	0.757
2.5	0.664	0.968	1.035
1000	0.249	0.249	0.249
10	0.249	0.469	0.464
2.5	0.249	0.399	0.391

initial momentums are selected to the momentum values corresponding to the dominant peaks in figures 1(a) and (b). It is found that the results obtained by the trajectory-based semiclassical analysis are almost consistent with those obtained by the DHW calculation.

On the other hand, we investigate the momentum spectra in figures 1(a) and (b) by employing the LDA method and compare them with the results obtained from the DHW formalism, as shown in figure 2. The red dashed line represents the result of the LDA. The main idea of this method is that when the spatial variation scale of the electric field is much larger than the Compton wavelength $\lambda \gg \lambda_C$, one can locally describe the pair production at any point x independently, which can be considered as occurring in a spatially homogeneous field $E(t)$ with field strength $E_0 f(x)$ [37, 42]. Therefore, the reduced momentum spectrum of created particles can be calculated by summing results for homogeneous field with different field strengths [31]:

$$\tilde{n}(p,\, t \to \infty) = \sum_x \frac{n(\epsilon(x)|p,\, t \to \infty)}{\lambda}, \tag{41}$$

where $n(\epsilon(x)|p,\ t \to \infty)$ represents the momentum distribution for the spatially homogeneous field $E(t)$ with field strength $\epsilon(x) = E_0 \exp\left(-\frac{x^2}{2\lambda^2}\right)$. It is noticed that the LDA method is suitable for the study of pair production at large spatial scales λ. Therefore, in figure 2, we select the results of $\lambda = 1000$ to compare and find that the results of the LDA are in good agreement with those of DHW calculation for $b = 0$ and $b = 3$.

3.1.2. Modulated frequency. When the modulated amplitude is fixed as $b = 0.1\omega/\omega_m = 1$, the momentum spectrum for different spatial scales with various modulated frequency ω_m is displayed in figure 3. It is noted that the results for $\omega_m = 0$ are the same as those for $b = 0$ in figure 1(a), which both indicate that the electric field is not modulated. At the large spatial scale $\lambda = 1000$, weak oscillations can be observed even for small modulated frequency, as shown in figures 3(a) and (b), which may be viewed as the interference effect between the created particles. Compared with the case of $\omega_m = 0$, the maximum peak values of the momentum spectra are increased by about 5 times. For large modulated frequency, one can see that strong oscillations appear, while the maximum peak values of the momentum spectra gradually decrease compared to the case of small modulation frequency, as shown in figures 3(c) and (d). This is confirmed by the corresponding frequency spectrum as illustrated in figure 4. On the other hand, compared with figure 1, it is found that the momentum spectrum in figure 3 has a good symmetry as the modulation frequency increases, while in figure 1, the symmetry of the spectrum is severely destroyed when the modulation amplitude becomes large. This indicates that the momentum spectrum is more sensitive to the modulated amplitude.

In order to see more clearly the variation of the maximum peak value of the momentum spectrum for different modulation frequencies in figure 3, we select the typical frequency spectra for $\omega_m = 0$ ($b = 0$), 0.07 and 0.1 to investigate, as shown in figure 4. Since in the quasihomogeneous limit, we can take the Fourier transform of the time dependence field $E(t) = E_0 \exp\left(-\frac{t^2}{2\tau^2}\right)\cos(\omega t + b\sin(\omega_m t))$, and obtain the corresponding frequency spectral structure. It is found that for $\omega_m = 0$, only one dominant frequency occurs on the Fourier spectrum, see figure 4(a), while for $\omega_m = 0.07$ and 0.1, there are not only one primary frequency but also two pairs of symmetrical subfrequencies on the spectra, see figures 4(b) and (c), which provide a great contribution to the external field frequency and lead to more energy to produce more particles. Particularly, the frequency spectrum structure consisting of combinations of ω_1, ω_2 and ω_3 and the spectrum structure consisting of combinations of ω_4, ω_5 and ω_6 can play a dynamically assisted role, which can significantly enhance the number of created particles. Therefore, we observed the maximum peak values of the momentum spectra in figures 3(b) and (d) are rapidly increased compared to the case of $\omega_m = 0$ in figure 1(a). It is noticed that for $\omega_m = 0.1$, the frequency spectrum structure is similar to the case of $\omega_m = 0.07$, and the difference is that the distance between each frequency component becomes further, see figure 4(c), which results in the decrease of the created particle number. Therefore, the maximum peak values of the momentum spectrum in figure 3(d) are smaller than the maximum peak values in figure 3(b). This is similar to the effect of time delay on the number of created particles. Previous studies have shown that a certain time delay reduces the number of created particles in the time delay external field [19].

In addition, we can use photon absorption to quantitatively understand the interference pattern of the typical momentum spectrum in figure 3. In the quasihomogeneous limit, the effective mass of a particle can be written as [38, 52]

$$m_* \approx m\sqrt{1 + \frac{E_0^2 m^2}{2\omega^2}}. \tag{42}$$

According to the definition of the total energy of the created

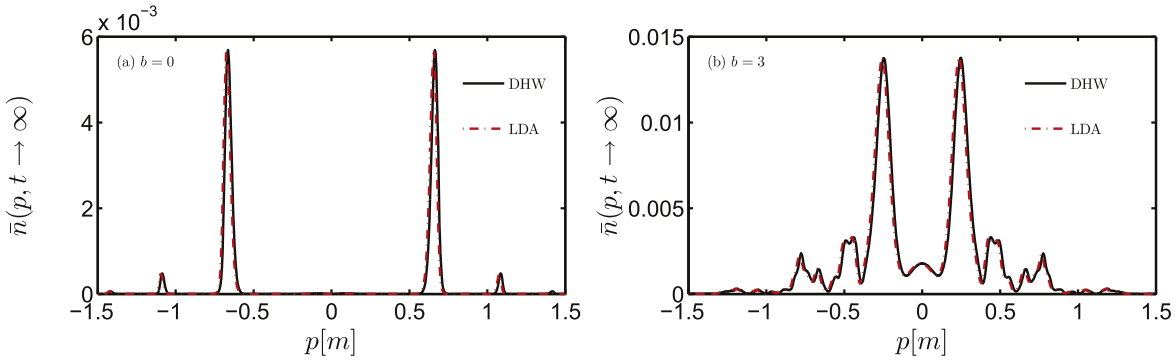

Figure 2. The momentum spectra of created particles with different modulated amplitude values calculated by DHW formalism and LDA for $\lambda = 1000$. Panel(a): The plot is for modulated amplitude $b = 0$. Panel(b): The plot is for modulated amplitude $b = 3$. Other field parameters are $E_0 = 0.3E_{\rm cr}$, $\omega = 0.5$, $\tau = 100$.

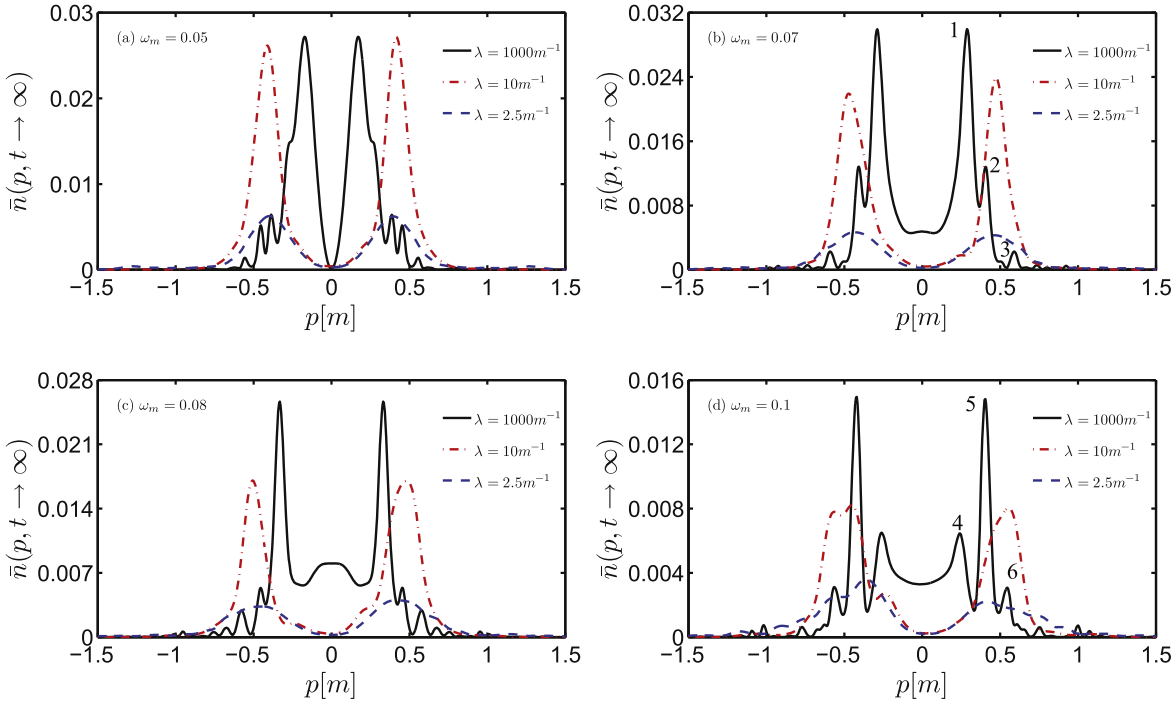

Figure 3. Reduced momentum spectrum for various modulated frequency values in electric field (38) with different spatial scales when modulated amplitude is $b = 1$. The modulated frequency values are $\omega_m = 0.05$, 0.07, 0.08 and 0.1, respectively. Other field parameters are the same as in figure 1.

particle, the total energy can be expressed as [38, 52]

$$E_p = 2\sqrt{m_*^2 + p^2} = n\omega. \tag{43}$$

The total energy E_1, E_2, ..., E_6 corresponding to the momentum peaks at p_1, p_2, ..., p_6 can be calculated by equation (43). For instance, in figure 3(b), when $p_1 = 0.288$, $p_2 = 0.405$ and $p_3 = 0.581$, we can obtain the corresponding total energy as $E_1 = 2.25 \approx 4\omega_2$, $E_2 = 2.32 \approx 3\omega_2 + \omega_3$ and $E_3 = 2.46 \approx 5\omega_1$, respectively. Therefore, we know that the momentum peaks at p_1, p_2, and p_3 correspond to 4-, 4- and 5-photon pair production. And the number of created particles by 4-photon absorption is much greater than that by 5-photon absorption. Meanwhile, it is found that $E_2 - E_1 = 0.07 = \omega_m$ and $E_3 - E_1 = 0.14 = 2\omega_m$, correspond to the frequency spectral structure in figure 4(b). For figure 3(d), when $p_4 = 0.244$, $p_5 = 0.405$ and $p_6 = 0.547$, the corresponding total energy $E_4 = 2.2 \approx 3\omega_4 + \omega_6$, $E_5 = 2.3 \approx 3\omega_5 + \omega_6$ and $E_6 = 2.4 \approx 5\omega_4$ are obtained according to equation (43). The momentum peaks at p_4, p_5, and p_6 are related to 4-, 4-, and 5-photon absorption. We also find that $E_5 - E_4 = 0.1 = \omega_m$ and $E_6 - E_4 = 0.2 = 2\omega_m$, which correspond to the frequency spectral structure in figure 4(c).

When the spatial scale reduces to $\lambda = 10$ and $\lambda = 2.5$, for small modulated frequency, there are no oscillations, but we can see that the momentum spectra present approximate symmetry, see figures 3(a) and (b). For large modulated frequency, we observe weak oscillations but the symmetry of the momentum spectrum is destroyed, as shown in figures 3(c) and (d). Moreover, there are some different phenomena on the momentum spectrum at $\lambda = 10$ and $\lambda = 2.5$. For $\lambda = 10$, compared to the case of $\lambda = 1000$, the dominant peaks of all the momentum spectra in figure 3 are

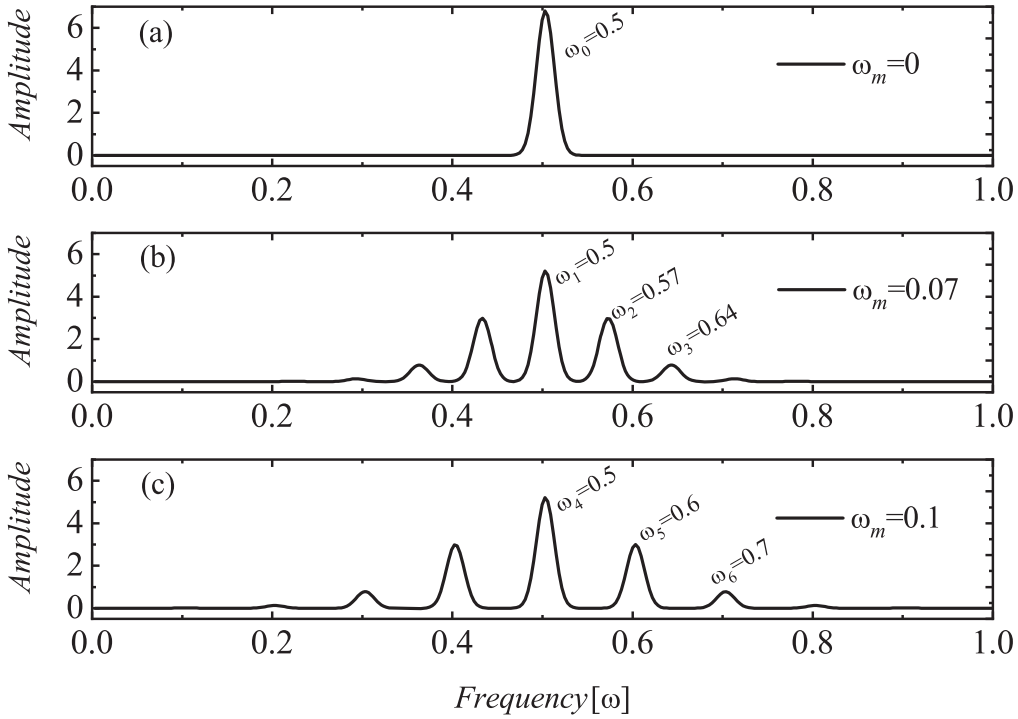

Figure 4. The frequency spectrum structure of time-dependent field with different modulated frequency values (a) $\omega_m = 0$, (b) $\omega_m = 0.07$ and (c) $\omega_m = 0.1$. Some typical values of frequency peaks are labeled on the panels. Other field parameters are $E_0 = 0.3E_{\rm cr}$, $\omega = 0.5$, $\tau = 100$, $b = 1$.

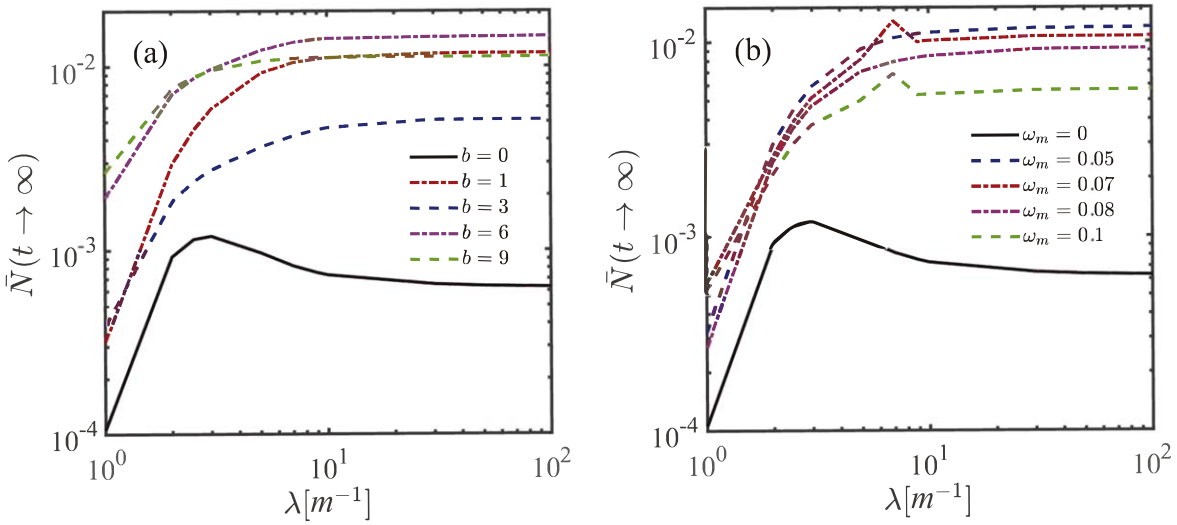

Figure 5. Reduced particle number dependence on spatial scales for different modulated frequency and amplitude parameters in electric field (38). Panel (a): The plot is for the change of modulated amplitude with $\omega_m = 0.05$. Panel (b): The plot is for the change of modulated frequency with $b = 1$. Other field parameters are the same as in figure 1.

shifted to the direction of large momentum, which can be explained by ponderomotive force [38]. Since the ponderomotive force is inversely proportional to the size of the spatial scale, i.e., the smaller the spatial scale, the stronger the ponderomotive force. Therefore, the dominant peaks of the momentum spectra at spatial scale $\lambda = 10$ are further pushed away from the center compared with the case of $\lambda = 1000$. For $\lambda = 2.5$, compared to the case of $\lambda = 10$, the momentum peaks are not pushed away from the center in figure 3. The highly inhomogeneous oscillation caused by the increase in modulation frequency decreases the corresponding effect of the ponderomotive force, which results in particles not being pushed into the regions of low field strength.

3.2. Reduced particle number

In this subsection, we study the effect of modulation parameters on the reduced particle number for various spatial scales, in different cases, such as modulating only in amplitude, modulating only in frequency, and modulating in both amplitude and frequency.

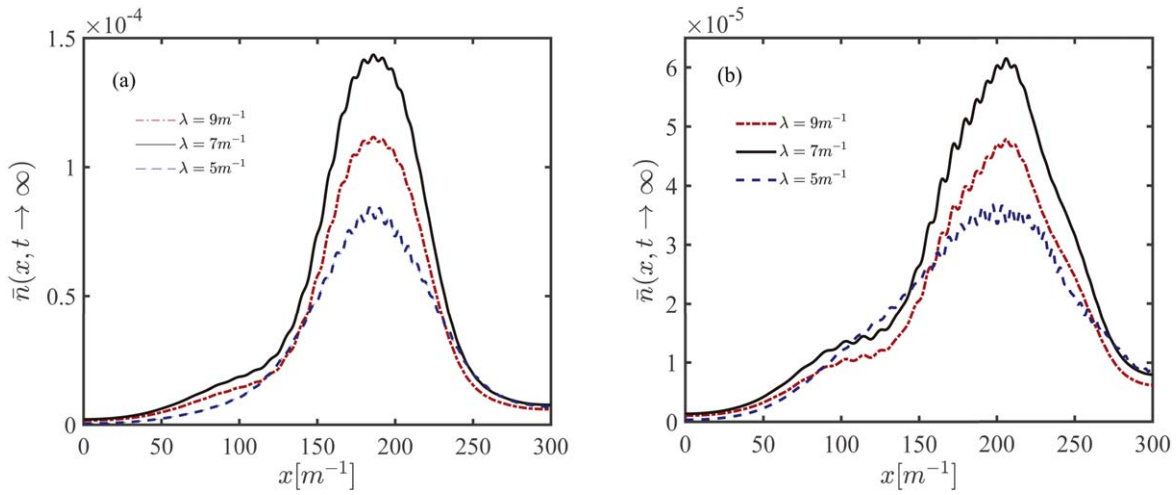

Figure 6. The position distribution for various spatial scales in electric field (38) with different modulated frequency values. The values are $\omega_m = 0.07$ for (a) and $\omega_m = 0.1$ for (b), respectively. Other field parameters are the same as in figure 5(b).

Figures 5(a) and (b) show the reduced particle number dependence on spatial scales for various modulated amplitude and frequency, respectively. It can be seen that when the spatial scale is fixed, the reduced particle number is significantly enhanced for various modulated amplitudes and frequencies. At large spatial scales, compared to the case of an electric field without modulation, the particle number is rapidly increased at about one order of magnitude by either the large modulated amplitude or small modulated frequency, as shown in figure 5. At small spatial scales, the enhancement of the particle number for various modulated amplitude and frequency is different. With increasing modulated amplitude, the particle number can be increased at about one order of magnitude, as shown in figure 5(a), while for modulated frequency, it is enhanced about 5 times, as shown in figure 5(b). Therefore, it indicates that the change of modulated amplitude is beneficial for pair production. Meanwhile, when the spatial scale is small, the particle number enhances rapidly with the spatial scale for small modulation amplitude, while it does not increase significantly for large modulation amplitude, as shown in figure 5(a). When the modulated amplitude is large, the particle production process is dominated by multiphoton absorption that is less influenced by the spatial scale.

When the modulation parameters (either the modulated amplitude or frequency) are fixed, with increasing spatial scale, the reduced particle number is rapidly increased at small spatial scales, while it tends to be a constant at large spatial scales. At small spatial scales, the electric field strength increases with the increase of the spatial scale, which results in more particles being created in the whole electric field region. It is noted that for certain modulated frequencies $\omega_m = 0.07$ and $\omega_m = 0.1$, the reduced particle number appears as an obvious nonlinear variation as spatial scale increases, i.e., there is a transition point at $\lambda = 7$, and the left and right sides of the transition point at $\lambda = 7$ correspond to $\lambda = 5$ and 9, respectively. It suggests that the reduced particle number is more sensitive to the modulation frequency than the modulation amplitude. Meanwhile, we can give some discussions on the transition point at $\lambda = 7$ employing the position distribution corresponding to $\lambda = 5$, 7, and 9, as shown in figure 6. It can be seen from figure 6(a), for $\omega_m = 0.07$, the largest peak and the broadest distribution are at $\lambda = 7$ in the position distribution, compared with the case of $\lambda = 5$ and 9. It indicates that more particles can be created in the position space when $\lambda = 7$. For $\omega_m = 0.1$, the phenomenon and discussion of figure 6(b) are similar to the case of figure 6(a).

Previous studies also have shown that, based on the relationship between the effective action and e^-e^+ pair production, for a purely time-dependent electric field, the faster the field changes (corresponding to a large frequency ω), the higher the pair production rate [53, 54]. In contrast, for a purely space-dependent electric field, the faster the field changes (corresponding to a small spatial scale λ), the lower the pair production rate[53]. Now it is noted that our electric field model equation(38) is composed of the space and time dependence, and we find that when $\omega_m = 0.07$ or $\omega_m = 0.1$, the variation of particle number with spatial scales is non-monotonic, as shown in figure 5(b). Since there is a delicate interaction between photon energy and field focusing [36, 38, 43] there is nonlinear variation in the pair production process. This is particularly interesting if our goal is to optimize the particle number within a given range of laser parameters. It can achieve a small total energy input by the laser but the number of created particles is large.

In order to study the effect of modulated frequency and amplitude on the reduced particle number more comprehensively, we present the contour plot, as shown in figure 7. Due to limited computational resources, we select an intermediate spatial scale $\lambda = 100$ for research, meanwhile, two significant features are revealed for the reduced particle number. One is that the same particle number can be achieved through different sets of modulation parameters. The other is that the reduced particle number is very sensitive to the modulation parameters, and the particle number from region I to region IV shows an obvious nonlinear variation, i.e., it goes from small to large and then from small to large. The reasons are as follows.

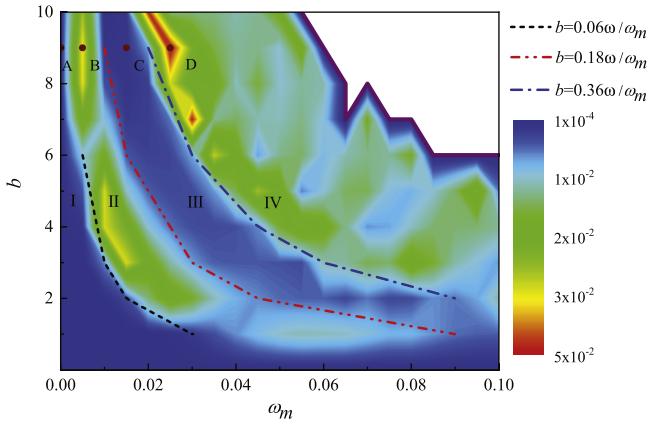

Figure 7. Contour plots of the reduced particle number versus the modulated frequency and amplitude at spatial scale $\lambda = 100$. Other field parameters are $E_0 = 0.3E_{cr}$, $\omega = 0.5$, $\tau = 100$. Note that the blank area separated by the purple solid line is beyond the modulation range of $\alpha = b\omega_m/\omega < 1$.

From figure 7, one can see that the four regions (I, II, III, IV) are divided by three typical curves, where these curves represent $b = 0.06\omega/\omega_m$, $b = 0.18\omega/\omega_m$ and $b = 0.36\omega/\omega_m$, respectively. It is noticed that there is an obvious hyperbolic relationship between modulated amplitude b and modulated frequency ω_m. The maximum effective frequency $\omega_{\text{eff}_{\max}} = \omega + b\omega_m = 0.53$ corresponds to the curve $b = 0.06\omega/\omega_m$, which is related to the 4-photon absorption process. The $\omega_{\text{eff}_{\max}} = 0.59$ corresponds to the curve $b = 0.18\omega/\omega_m$, which also corresponds to 4-photon absorption. However, the $\omega_{\text{eff}_{\max}} = 0.68$ corresponds to the curve $b = 0.36\omega/\omega_m$, which is related to the 3-photon absorption process. Therefore, the pair production processes in regions I, II, and III correspond to 4-photon absorption, while it is related to 3-photon absorption in regions IV. It is well known that the number of created particles by 3-photon absorption is much greater than that by 4-photon absorption, thus the reduced particle number is significantly enhanced in regions IV. However, for regions I, II, and III, there should not be much difference in the corresponding number of created particles, since the pair production processes all belong to 4-photon absorption, but the particle number in regions II is larger with respect to the regions I and III. This result is very interesting, though it is counterintuitive, but can be understood by the frequency spectrum structure in figure 8.

To facilitate understanding of this counterintuitive result, we select the four typical points A, B, C, and D of regions I, II, III, and IV in figure 7, respectively, and give the frequency spectrum structures corresponding to these points, as shown in figure 8. It can be seen from figure 8(a), there is only one primary frequency $\omega = 0.5$ on the frequency spectrum, while in figure 8(b), in addition to the primary frequency, two secondary frequencies appear in the spectral structure and the amplitude of the spectrum is almost the same as the case of figure 8(a), but the primary frequency is increased to $\omega = 0.545$. Therefore, the particle number corresponding to point B is larger than that of point A, as shown in table 3. Meanwhile, from figure 8(c), it is found that there are more frequency components on the spectral structure, and the dominant frequency is increased to $\omega = 0.635$, but the amplitude is reduced by almost half compared to the case of figure 8(b). Since in figures 8(b) and (c), the corresponding dominant frequencies are $\omega = 0.545$ and $\omega = 0.635$, respectively, the pair production process is related to 4-photon absorption. But the amplitude is significantly reduced in figure 8(c), which leads to a rapid decrease in the electric field strength. Therefore, the particle number corresponding to point B is significantly larger than that of point C, as shown in table 3. While in figure 8(d), we observe that there are many frequency components on the frequency spectrum, and the dominant frequency is increased to near the $\omega = 0.7$, which means the pair production process is related to 3-photon absorption. Therefore, the particle number corresponding to point D is larger than that of A, B, and C, as shown in table 3.

To study whether there are optimal modulation parameters for e^-e^+ pair production in a spatial inhomogeneous field with sinusoidal phase modulation, we further explore the variation of the reduced particle number in the following two cases at spatial scale $\lambda = 100$, as shown in figure 9(a). One case is that the electric field does not have any modulation, only the central frequency ω. The other case is that the electric field has both central frequency and modulation, where the central frequency is $\omega = 0.5$, and the modulation is that the modulated frequency is fixed $\omega_m = 0.01$, but the modulated amplitude b changes. It is found that the trends of the results in the above two cases are almost identical. In the second case, we perform the Fourier transform of the time-dependent electric field and regard the frequency with the largest amplitude on the frequency spectrum as the original center frequency of the electric field without modulation, which makes the trends almost identical. Moreover, in the first case, it is found that the reduced particle number is extremely sensitive to the central frequency of the external field and presents an obvious nonlinear variation. In particular, when the central frequency is $\omega = 0.69$, the particle number reaches the maximum value, i.e., $\bar{N} = 0.1331$, and it is significantly enhanced by more than two orders of magnitude compared to the case without modulation, i.e., $\omega = 0.5$. In the second case, we can also observe the sensitivity of the reduced particle number to the modulated amplitude and find that when modulated frequency $\omega_m = 0.01$ and modulated amplitude $b = 20.7$, the reduced particle number reaches the maximum value, i,e., $\bar{N} = 0.1367$, which is almost the same as the maximum value in the first case.

Figure 9(b) shows the change in the ratio of the reduced particle number in the above two cases and the particle number under the electric field without modulation. In the first case, one can see that when the central frequency of the external field is $\omega = 0.69$, the ratio reaches the maximum value, i.e., $\bar{N}(b = 0)/\bar{N}(\omega = 0.5, b = 0) \approx 211$, while in the second case, when modulated frequency $\omega_m = 0.01$ and modulated amplitude $b = 20.7$, the maximum value of the ratio is $\bar{N}(\omega_m = 0.01)/\bar{N}(\omega = 0.5, b = 0) \approx 217$. It indicates that in the two cases, the reduced particle numbers are significantly enhanced about 200 times compared to the case without modulation, i.e., $\omega = 0.5$. Therefore, we can obtain that $\omega = 0.69$ is the optimal value of the central frequency of the external field to

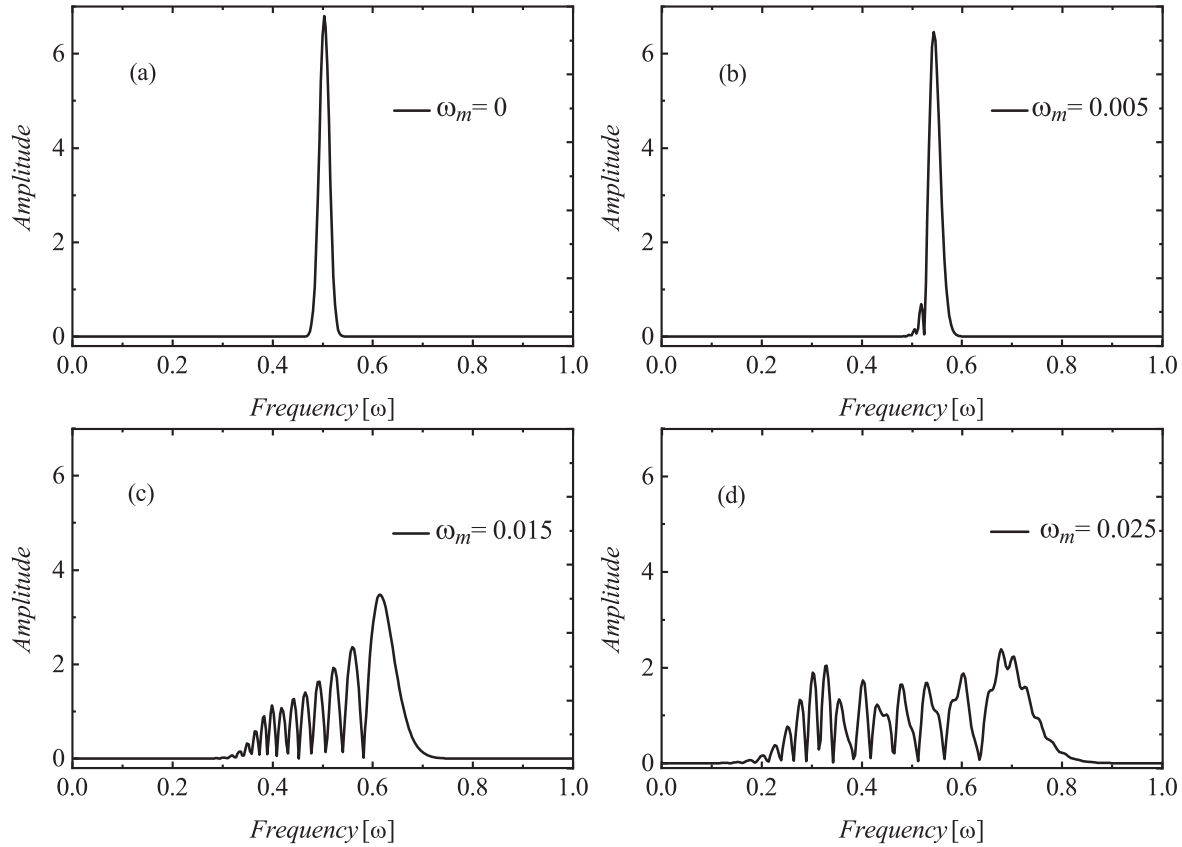

Figure 8. The frequency spectrum structure for different points A, B, C and D marked in figure 7. The corresponding modulation parameters are (a) $\omega_m = 0$, (b) $\omega_m = 0.005$, (c) $\omega_m = 0.015$ and (d) $\omega_m = 0.025$ with $b = 9$. Other field parameters are $E_0 = 0.3E_{\rm cr}$, $\omega = 0.5$, $\tau = 100$.

Table 3. The reduced particle number for the points marked in figure 7 with different modulation regions.

Modulation region	Modulation parameters (ω_m, b)	Reduced particle number
I	A(0, 9)	6.30×10^{-4}
II	B(0.005, 9)	3.42×10^{-2}
III	C(0.015, 9)	1.99×10^{-3}
IV	D(0.025, 9)	4.54×10^{-2}

get the largest reduced particle number, meanwhile, $\omega_m = 0.01$ and $b = 20.7$ are the optimal values of the modulated frequency and the modulated amplitude to get the largest reduced particle number.

4. Conclusion and outlook

In summary, with the DHW formalism, we have investigated the sinusoidal phase modulation effects on the momentum spectrum and the reduced particle number in inhomogeneous fields. The effect of the spatial scale of the external field on the pair production is further examined. Meanwhile, some typical interference patterns of momentum spectra are quantitatively analyzed by bridging momentum peaks and the corresponding frequency spectra. Moreover, we compared some typical numerical results obtained by the DHW formalism with those obtained by the trajectory-based semiclassical analysis method and the LDA method. It is found that they are in good agreement.

For the momentum spectrum, a significant interference effect occurs with the increase of either modulated amplitude or frequency. Moreover, the larger amplitude modulation leads to an asymmetry of the momentum spectrum, while the frequency modulation keeps a good symmetry of the momentum spectrum.

For the reduced particle number, it is significantly enhanced by the variation of modulation parameters for different spatial scales. At small spatial scales, compared with the case without modulation, the particle number is enhanced by more than one order of magnitude with modulated amplitude, while it is increased about 5 times with modulated frequency. At large spatial scales, the particle number is increased by more than one order of magnitude with modulation parameters. When modulation parameters are fixed, the reduced particle number increases rapidly with the increase of spatial scale at small spatial scales, while it tends to be a constant at large spatial scales.

Importantly, it is found that the particle number at small spatial scales is larger than that in the case of large spatial scales when modulation parameters are fixed ($\omega_m = 0.07$ and 0.1). It indicates that the total energy input by the laser is small, but the number of created particles is large. Therefore, our electric field model provides a possibility to achieve high efficiency e^-e^+ pair production. Moreover, it is found that for an obtained particle number, it can be achieved by different sets of modulation parameters when spatial scales are fixed.

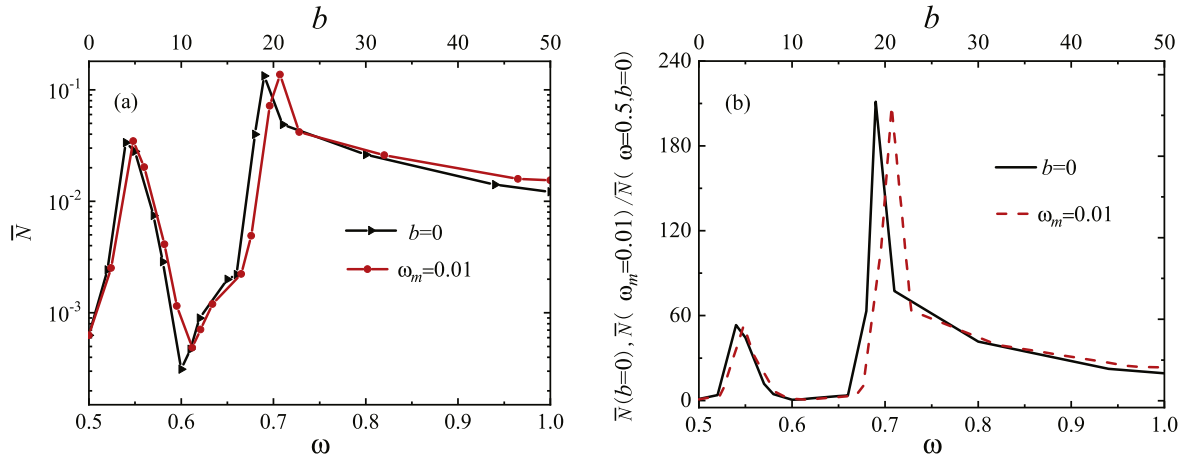

Figure 9. (a) Reduced particle number as a function of the central frequency of the external field (black line) when $b = 0$ and the modulated amplitude (red line) when $\omega_m = 0.01$ is fixed at spatial scale $\lambda = 100$, respectively. Other field parameters are $E_0 = 0.3E_{\rm cr}$, $\omega = 0.5$, $\tau = 100$. (b) The ratio of $\bar{N}(b = 0)/\bar{N}(\omega = 0.5, b = 0)$, $\bar{N}(\omega_m = 0.01)/\bar{N}(\omega = 0.5, b = 0)$ as a function of the central frequency (black line) and the modulated amplitude (red line), respectively.

This is important since it can provide more freedom in parameter selection for pair production. Therefore, by combining the above two effects of the spatial scale in inhomogeneity of the fields and the different ways of modulation, we can effectively achieve the optimal pair production with the more flexible parameter selection.

Our study indicates that the sinusoidal phase modulation would play a crucial role in e^-e^+ pair production under spatially inhomogeneous electric fields, meanwhile, it also provides a possibility of broader parameter ranges for realizing the optimal pair production. While we have only considered e^-e^+ pair production in a single field, it is believed that the presented scheme about the phase modulation can be extended to the case of multiple fields, in which the dynamically assisted effect is included.

Acknowledgments

We thank Li Wang and MA Bake for the fruitful discussions and their help with the numerical calculation. This work was supported by the National Natural Science Foundation of China (NSFC) under Grant No. 11 875 007 and No. 11 935 008. The computation was carried out at the HSCC of the Beijing Normal University.

ORCID iDs

B S Xie https://orcid.org/0000-0003-0757-9134

References

[1] Sauter F 1931 Uber das Verhalten eines elektrons im homogenen elektrischen feld nach der relativistischen theorie Diracs *Z. Phys.* **69** 742
[2] Heisenberg W and Euler H 1936 Folgerungen aus der Diracschen theorie des positrons *Z. Phys.* **98** 714
[3] Di Piazza A, Muller C, Hatsagortsyan K Z and Keitel C H 2012 Extremely high-intensity laser interactions with fundamental quantum systems *Rev. Mod. Phys.* **84** 1177
[4] Fedotov A, Ilderton A, Karbstein F, King B, Seipt D, Taya H and Torgrimsson G 2022 Advances in QED with intense background fields arXiv:2203.00019
[5] Schwinger J S 1951 On Gauge invariance and vacuum polarization *Phys. Rev.* **82** 664
[6] Dunne G V 2009 New strong-field QED effects at extreme light infrastructure *Eur. Phys. J.* D **55** 327
[7] Burke D L *et al* 1997 Positron production in multi-photon light by light scattering *Phys. Rev. Lett.* **79** 1626
[8] Bamber C *et al* 1999 Studies of nonlinear QED in collisions of 46.6-GeV electrons with intense laser pulses *Phys. Rev.* D **60** 092004
[9] Narozhny N B, Bulanov S S, Mur V D and Popov V S 2004 On e^+e^- pair production by colliding electromagnetic pulses *JETP* **80** 382
[10] Fedotov A M 2009 Electron-positron pair creation by a strong tightly focused laser field *Laser Phys.* **19** 214
[11] Schutzhold R, Gies H and Dunne G 2008 Dynamically assisted Schwinger mechanism *Phys. Rev. Lett.* **101** 130404
[12] Abdukerim N, Xie B S, Li Z L and Dulat S 2013 Electron-positron pair production in a strong laser field enhanced by an assisted high frequency weak field *Commun. Theor. Phys.* **59** 331
[13] Ibrahim S, Li Z L and Xie B S 2017 Electron-positron pair production in strong fields characterized by conversion energy *Commun. Theor. Phys.* **67** 76
[14] Bulanov S S, Mur V D, Narozhny N B, Nees J and Popov V S 2010 Multiple colliding electromagnetic pulses: a way to lower the threshold of e^+e^- pair production from vacuum *Phys. Rev. Lett.* **104** 220404
[15] Li Z L, Lu D and Xie B S 2015 Dynamically assisted pair production for scalar QED by two fields *Front. Phys.* **10** 101201
[16] Di Piazza A, Lotstedt E, Milstein A I and Keitel C H 2009 Barrier control in tunneling e^+-e^- photoproduction *Phys. Rev. Lett.* **103** 170403
[17] Ringwald A 2001 Pair production from vacuum at the focus of an X-ray free electron laser *Phys. Lett.* B **510** 107
[18] Li Z L, Lu D, Xie B S, Fu L B, Liu J and Shen B F 2014 Enhanced pair production in strong fields by multiple-slit interference effect with dynamically assisted Schwinger mechanism *Phys. Rev.* D **89** 093011

[19] Li Z L, Li Y J and Xie B S 2017 Momentum vortices on pairs production by two counter-rotating fields *Phys. Rev.* D **96** 076010
[20] Mohamedsedik M, Xie B S and Dulat S 2012 Analytical study of pair production rate from vacuum in an elliptic polarized field by a two-level transition technique *Commun. Theor. Phys.* **57** 422
[21] He L Y, Xie B S, Guo X H and Wang H Y 2012 Electron-positron pair production in an arbitrary polarized ultrastrong laser field *Commun. Theor. Phys.* **58** 863
[22] Nuriman A, Li Z L and Xie B S 2015 Electron-positron pair production in the low-density approximation *Front. Phys.* **10** 101202
[23] Jia M R, Li Z L, Lv C, Wan F and Xie B S 2017 Pair production in strong SU(2) background fields *Front. Phys.* **12** 121101
[24] Hebenstreit F, Alkofer R, Dunne G V and Gies H 2009 Momentum signatures for Schwinger pair production in short laser pulses with sub-cycle structure *Phys. Rev. Lett.* **102** 150404
[25] Nuriman A, Xie B S, Li Z L and Sayipjamal D 2012 Enhanced electron-positron pair creation by dynamically assisted combinational fields *Phys. Lett.* B **717** 465
[26] Dumlu C K and Dunne G V 2011 Interference effects in Schwinger vacuum pair production for time-dependent laser pulses *Phys. Rev.* D **83** 065028
[27] Oluk O, Xie B S, Bake M A and Dulat S 2014 Electron-positron pair production in a strong asymmetric laser electric field *Front. Phys.* **9** 157
[28] Strickland D and Mourou G 1985 Compression of amplified chirped optical pulses *Opt. Commun.* **55** 447
[29] Dumlu C K 2010 Schwinger vacuum pair production in chirped laser pulses *Phys. Rev.* D **82** 045007
[30] Olugh O, Li Z L, Xie B S and Alkofer R 2019 Pair production in differently polarized electric fields with frequency chirps *Phys. Rev.* D **99** 036003
[31] Ababekri M, Sayipjamal Dulat, Xie B S and Zhang J 2020 Chirp effects on pair production in oscillating electric fields with spatial inhomogeneity *Phys. Lett.* B **810** 135815
[32] Li L J, Mohamedsedik M and Xie B S 2021 Enhanced dynamically assisted pair production in spatial inhomogeneous electric fields with the frequency chirping *Phys. Rev.* D **104** 036015
[33] Wang K, Hu X H, Dulat S and Xie B S 2021 Effect of symmetrical frequency chirp on pair production *Chin. Phys.* B **30** 060204
[34] Mohamedsedik M, Li L J and Xie B S 2021 Schwinger pair production in inhomogeneous electric fields with symmetrical frequency chirp *Phys. Rev.* D **104** 016009
[35] Gong C, Li Z L, Xie B S and Li Y J 2020 Electron-positron pair production in frequency modulated laser fields *Phys. Rev.* D **101** 016008
[36] Kohlfürst C 2020 Effect of time-dependent inhomogeneous magnetic fields on the particle momentum spectrum in electron-positron pair production *Phys. Rev.* D **101** 096003
[37] Hebenstreit F, Alkofer R and Gies H 2011 Particle self-bunching in the Schwinger effect in spacetime-dependent electric fields *Phys. Rev. Lett.* **107** 180403
[38] Kohlfürst C and Alkofer R 2018 Ponderomotive effects in multiphoton pair production *Phys. Rev.* D **97** 036026
[39] Kohlfürst C 2018 Phase-space analysis of the Schwinger effect in inhomogeneous electromagnetic fields *Eur. Phys. J. Plus* **133** 191
[40] Ababekri M, Xie B S and Zhang J 2019 Effects of finite spatial extent on Schwinger pair production *Phys. Rev.* D **100** 016003
[41] Aleksandrov I A and Kohlfürst C 2020 Pair production in temporally and spatially oscillating fields *Phys. Rev.* D **101** 096009
[42] Li Z L, Gong C and Li Y J 2021 Study of pair production in inhomogeneous two-color electric fields using the computational quantum field theory *Phys. Rev.* D **103** 116018
[43] Kohlfürst C 2015 Electron-positron pair production in inhomogeneous electromagnetic fields *PhD thesis* arXiv:1512.06082
[44] Hebenstreit F 2011 Schwinger effect in inhomogeneous electric fields *PhD thesis* arXiv:1106.5965
[45] Brezin E and Itzykson C 1970 Pair production in vacuum by an alternating field *Phys. Rev.* D **2** 1191
[46] Kim S P and Page D N 2007 Improved approximations for fermion pair production in inhomogeneous electric fields *Phys. Rev.* D **75** 045013
[47] Strobel E and Xue S S 2015 Semiclassical pair production rate for rotating electric fields *Phys. Rev.* D **91** 045016
[48] Oertel J and Schützhold R 2019 WKB approach to pair creation in spacetime-dependent fields: the case of a spacetime-dependent mass *Phys. Rev.* D **99** 125014
[49] Dumlu C K and Dunne G V 2010 Stokes phenomenon and Schwinger vacuum pair production in time-dependent laser pulses *Phys. Rev. Lett.* **104** 250402
[50] Silenko A J 2008 Foldy-wouthyusen transformation and semiclassical limit for relativistic particles in strong external fields *Phys. Rev.* A **77** 012116
[51] Wen M, Bauke H and Keitel C H 2016 Identifying the Stern-Gerlach force of classical electron dynamics *Sci. Rep.* **6** 31624
[52] Kohlfürst C, Gies H and Alkofer R 2014 Effective mass signatures in multiphoton pair production *Phys. Rev. Lett.* **112** 050402
[53] Gies H and Klingmuller K 2005 Pair production in inhomogeneous fields *Phys. Rev.* D **72** 065001
[54] Linder M F, Schneider C, Sicking J, Szpak N and Schützhold R 2015 Pulse shape dependence in the dynamically assisted Sauter-Schwinger effect *Phys. Rev.* D **92** 085009